

Curve	Investigator	Aspect ratio	Reynolds Number	Comments
a	Ideal fluid	∞	∞	
b	Thom	12.5 and 26	5 300 - 8 800	End disks 3ϕ
c	Reid	13.3	39 000 - 116 000	
d	Gottingen	4.7	52 000	End disks 1.7ϕ
e	Thom	8	16 000	
f	Swanson	∞	35 000 - 300 000	
g	Thom	5.7	30 000 - 90 000	Rough surface (sanded)
h	Thom	5.7	30 000 - 90 000	Smooth surface
i	Gottingen	4.7	52 000	
j	Schwarzenberg	4.5	54 000, 186 000	Unpublished
k	Swanson	2	53 000	Continuous end sections

Fig. 1.1. Lift on a rotating cylinder (taken from Swanson (1961))

From the above figure it is clear that as the aspect ratio increases the lift curve tends to that of the theoretical prediction for an ideal fluid labelled a.

This paper considers the two dimensional Magnus forces in detail. Two of the conclusions are that the smaller the aspect ratio the smaller the maximum lift obtained and the smaller the velocity ratio at which it occurs. Swanson claims that leakage flow and the consequent effects are responsible for the aspect ratio effect. For this reason the experimenters went to great lengths to eliminate these effects. Some of the methods used were end plates, segmented cylinders and projecting the cylinder out of the wind tunnel walls. The use of end plates resulted in a complex flow resulting from finite cylinder flow and end plate effects combined. This was not similar to the flow over an infinite cylinder. Swanson in this same paper gives results of tests carried out by himself using a segmented cylinder. The cylinder consisted of three segments linked by linkages that transmitted torque and minimal forces. The two outer segments projected out of the wind tunnel and the forces were only measured on the central segment. Although the data presented below only shows results up to a velocity ratio of one, Swanson carried out tests up to a velocity ratio of 17 and the Lift did not demonstrate the maximum predicted by Prandtl. The following three graphs use a common legend table given after figure 7.4.

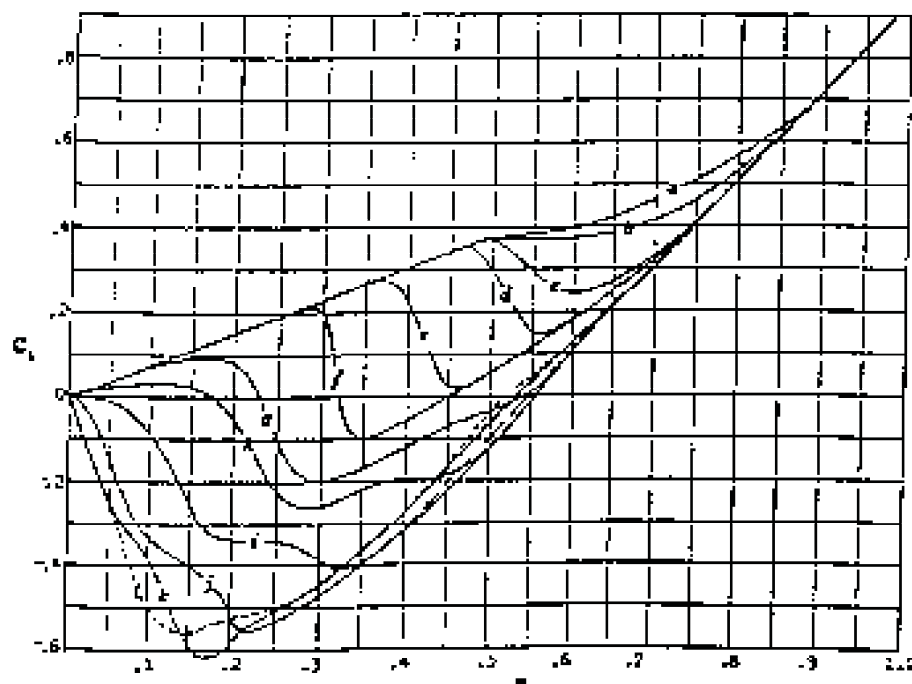


Fig. 3.2. Lift variation with velocity ratio from Swanson (1961).
Graph 1

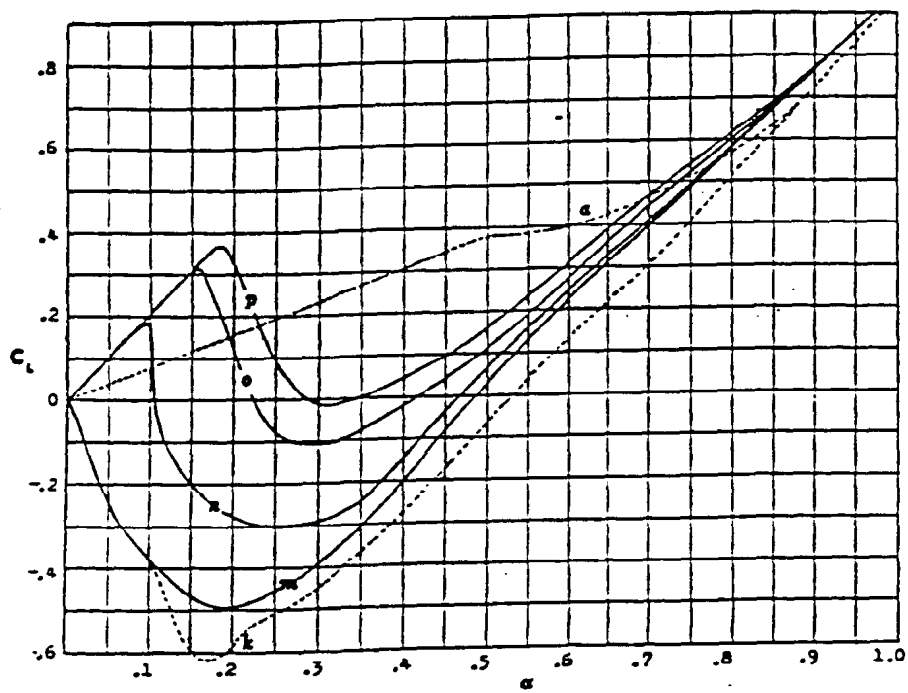


Fig. 3.3.

Lift variation with velocity ratio from Swanson (1961).

Graph 2

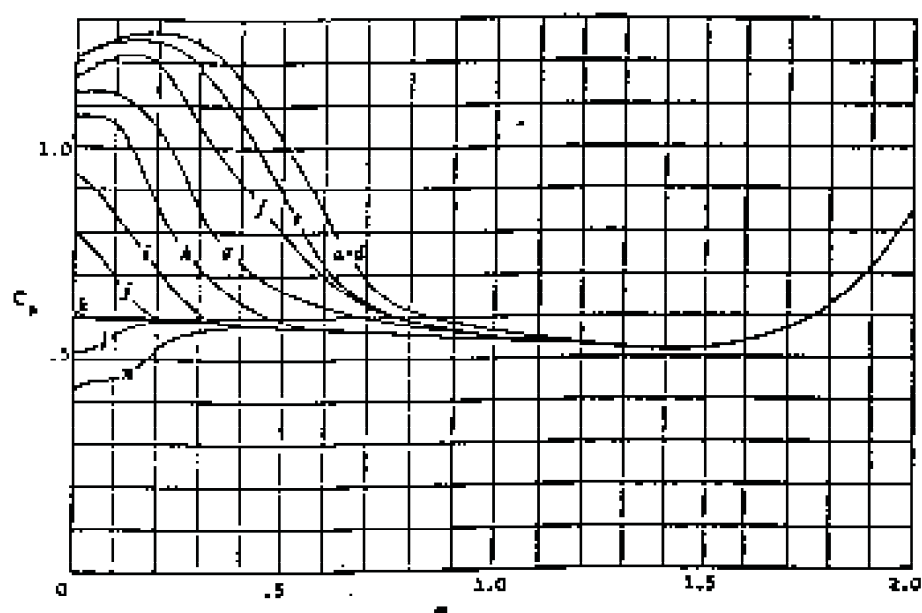


Fig. 3.4. Drag variation with velocity ratio from Swanson (1961)

Curve Designation	Reynolds Number
a	35 800
b	49 000
c	60 700
d	79 100
e	99 000
f	128 000
g	152 000
h	181 500
i	225 000
j	260 000
k	295 000
l	325 000
m	365 000
n	420 000
o	450 000
p	501 000

3.4 THEORETICAL AND NUMERICAL ANALYSES OF SPHERES

Hannulec published three papers (1963, 1967, 1967) and co-authored one (1970) on the numerical analysis of the flow over fluid spheres for the chemical industry. This work was limited to low Reynolds numbers, less than 500 for the first two papers and less than 200 for the third. The first paper (1963) compared the results he obtained with those measured experimentally. In the first of a two part publication (1967) it was undertaken to establish the accuracy of a finite difference method solving the Navier-Stokes equations. The conclusion of this publication was that the computer time required to obtain more than 8% accuracy did not warrant the effort.

Singh (1975) worked on the flow past a spinning sphere. The conditions considered were rotating flow at low Reynolds numbers.

Zapryanov (1977) investigated the growth of the boundary layer on a spinning sphere.

Rubinow and Keller (1961) formulated a model to predict the three forces on a spinning sphere, and the torsion due to viscous effects. The model uses the Stokes and Oseen expansions which are only accurate at Reynolds numbers of order 1. Some researchers state that the accuracy of such analyses are acceptable up to Reynolds numbers of 100. The formulae for Lift and Drag are given below

$$C_L = 2a[1 + O(Re)]$$

$$C_D = \frac{12\mu}{\rho V_\infty} \left[1 + \frac{3}{8} Re + o(Re) \right]$$

3.5 EXPERIMENTAL STUDIES ON THE FLOW OVER STATIONARY SPHERES

The earliest reference on vortex shedding (Cometta 1957) measured the Von Karman vortex street behind both spheres and cylinders using hot wire techniques. At the same time the wake region was being studied by Taneda (1956). He established the relationship between vortex ring size and Reynolds number. He also established the relationship between the separation angle and Reynolds number. Taneda worked in the range of $Re = 3$ to $Re = 300$.

Maxworthy (1968) experimented with a sphere being drawn through a rotating tank of viscous fluid. He measured the drag and flow profile.

Calvert (1970) found that by tripping the boundary layer, vortices were no longer shed regularly.

Achenbach (1972) undertook work on the flow over spheres at very high Reynolds numbers, typically 50 000 and 600 000. His work covered both force measurements and flow analysis. He later went on to determine the mechanisms of vortex shedding. Use was made of a hot wire probe on the surface of the sphere that could be rotated circumferentially. The three dimensional schematic of the vortex behind a sphere Achenbach proposed is very different from that proposed by Pao and Kao (1977). Both schematics were for flow at a Reynolds number of 1000. Both authors had similar shapes just behind the sphere. The vortex formation at high Reynolds numbers was investigated by Taneda (1978).

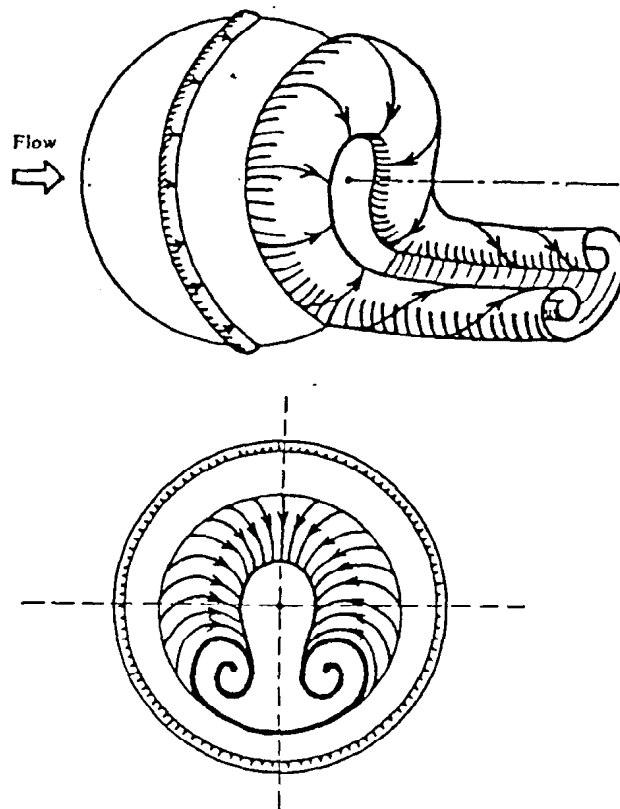


Fig. 3.5.

Schematic representation of the vortex Structure behind a stationary sphere at $Re = 380\,000$ as presented by Taneda (1978).

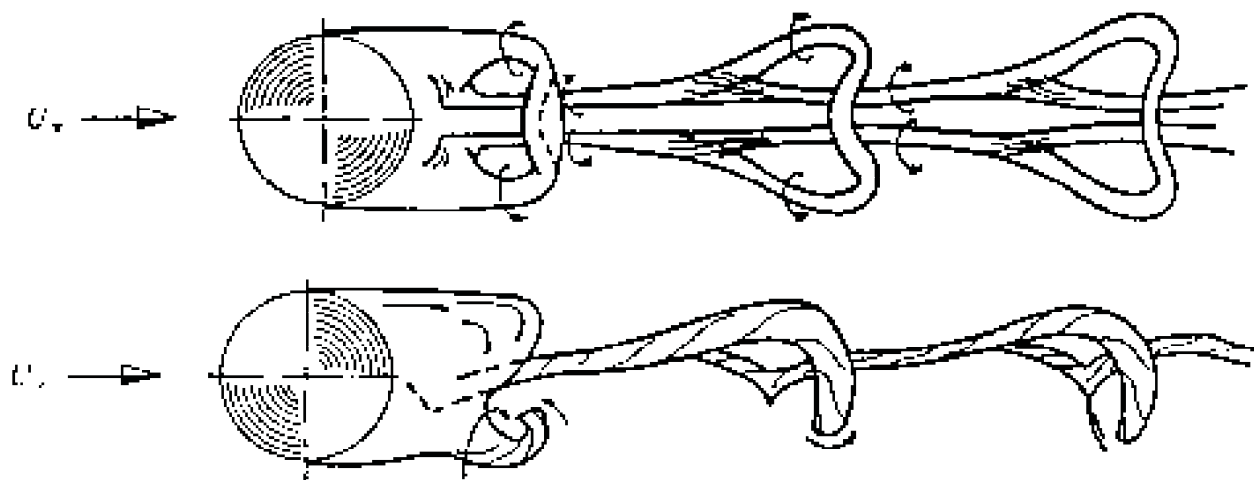


Fig. 3.6. Schematic representation of the vortex configuration in the wake of a stationary sphere at $Re = 1000$ as presented by Achenbach (1972).

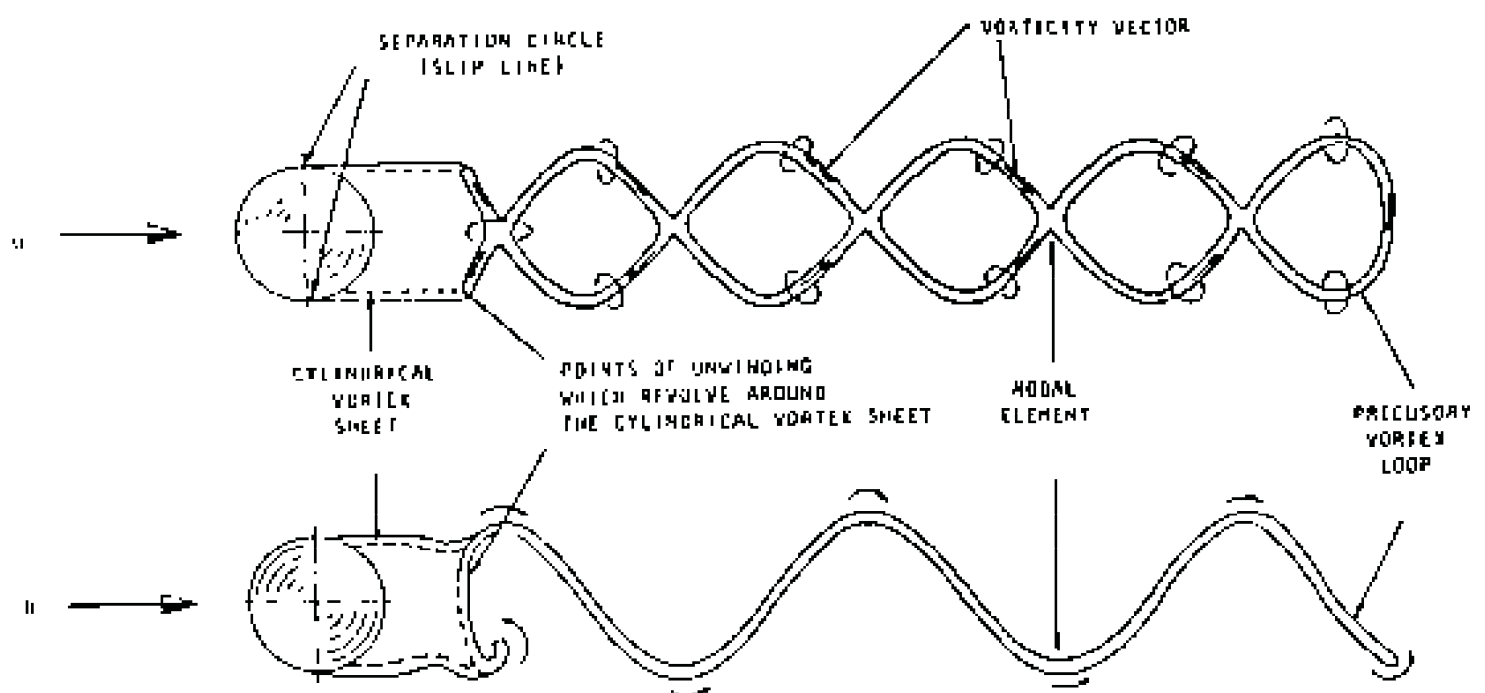


Fig. 3.7. Schematic representation of the vortex configuration in the wake of a stationary sphere at $Re = 1000$ as presented by Pan and Kao (1977).

Boundary layer experimentation was carried out by Seeley et al (1975). His work was limited to intermediate Reynolds numbers. The results were recorded on film and measurements were made by advancing the film frame by frame. Eismail et al (1979) re-processed his results using a Polly film reading system resulting in better accuracy.

4 EXPERIMENTAL EQUIPMENT

The experimental equipment used is divided into four major categories with supplementary pieces of apparatus. The four main categories are:

- 1) The Wind Tunnel
- 2) The Six Component Sting Balance
- 3) The Model
- 4) The Data Acquisition System

Each section is discussed individually.

4.1 THE WIND TUNNEL

The wind tunnel was an open circuit tunnel with a square test section. The dimensions of the test section were 1.5 m square with 300 mm fillets on the corners and a length of 8 m. The maximum velocity in the tunnel was 20 m/s if the density at the time of testing was not too high. There was honeycomb flow straightener on either end of the test section where it connected with the inlet and diffuser. There was also approximately 5m between the flow straightener at the nozzle and the model to allow the flow to settle.

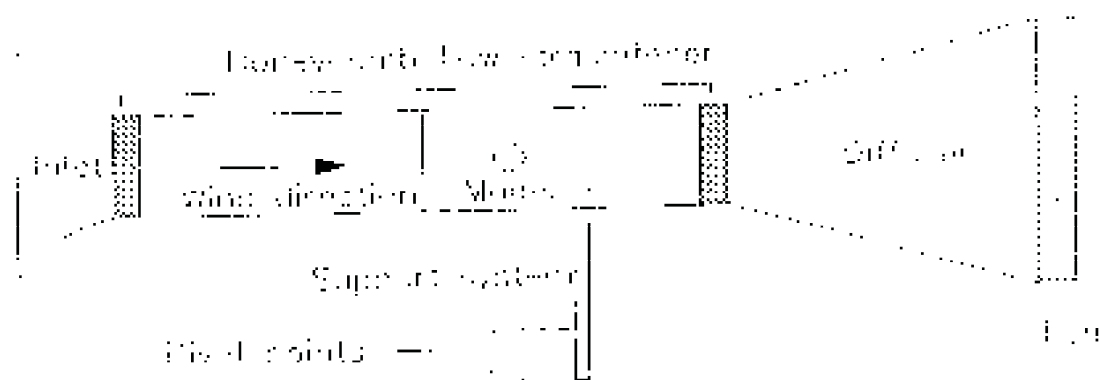


Fig.4.1. Schematic of the wind tunnel.

The fan was directly in front of the diffuser. The diffuser was facing a brick wall with a distance of four metres between them, which is thought to be the cause of vibrational problems. The tunnel was subsequently modified to duct the flow directly out of the building.

The design of the tunnel was modular and made of wood supported by a steel frame. The reason for this is to allow for different test sections to be built and wheeled into place cheaply should this be required.

The sting and model assembly was mounted on a turn-table that could rotate about its central axis through 180° . This meant that the model could be rotated from -90° to 90° relative to the flow direction in the horizontal plane. The model was mounted on a sting balance that could pitch from -30° to 30° . The model also remained in the same place throughout a test even when the pitch and yaw angles were changed. This was achieved by using a parallelogram support structure (support A). The angles could be read directly into the data acquisition system by means of a potentiometer in a Wheatstone bridge configuration. The angles were measured by a closed loop system. This meant that the potentiometer is independent of the setting mechanism and therefore measures the resultant and not the applied setting. The angle of attack could be changed using a worm gearbox with a ratio of 100 : 1. The yaw angle was changed either manually, by physically rotating the table, or by rotating a handle which operated a chain drive to turn the table.

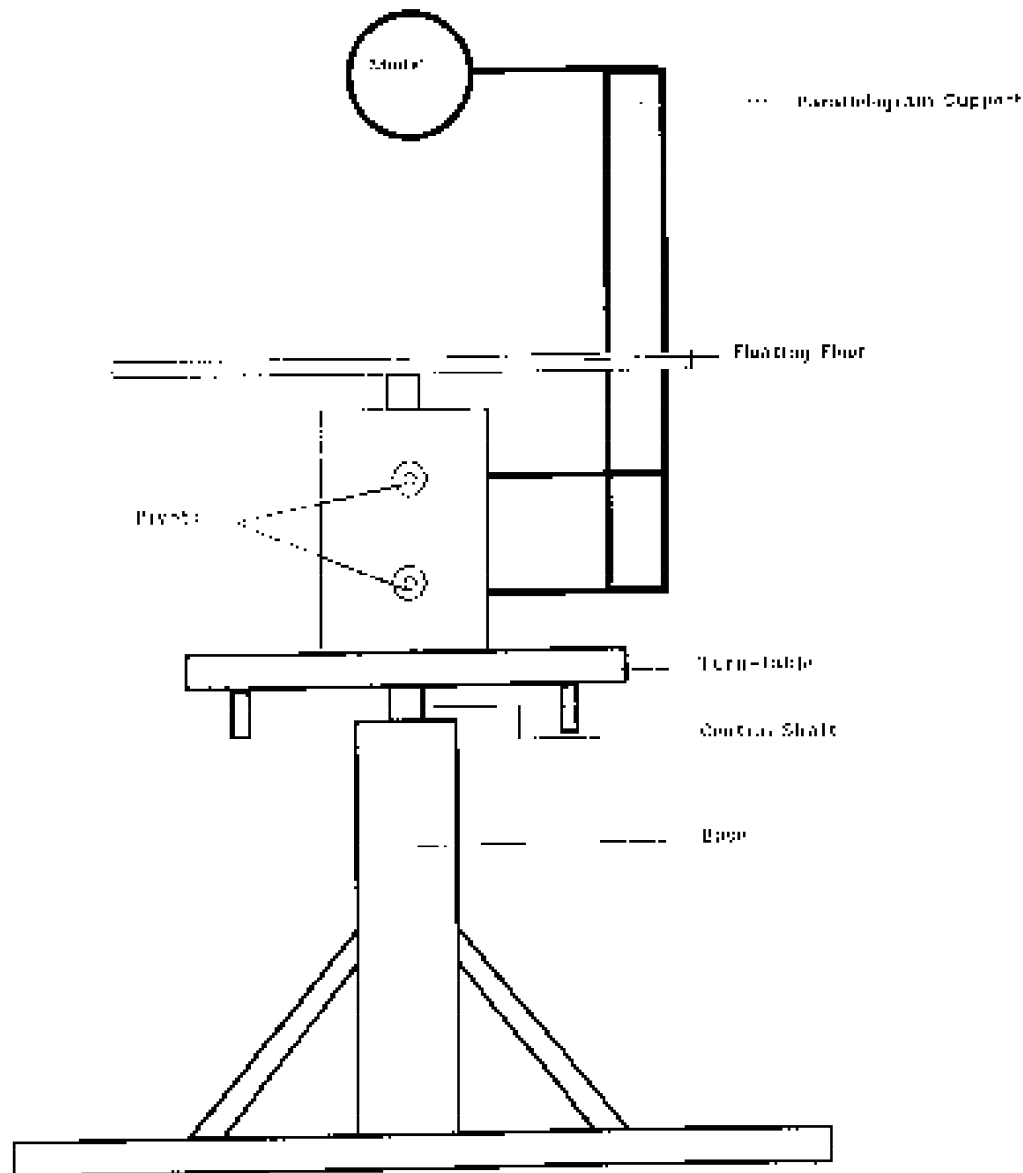


Fig 4.2. Schematic of Support A.

The uprights in the parallelogram support were made of circular tubing with as small a diameter as possible so that the interference effects would be as small as possible. These tubes were originally made of aluminium but were subsequently changed to stainless steel to give more rigidity.

Once the first set of tests had been completed and processed it was feared that the fluctuation noted was due to the lack of stiffness in the support. For this reason a second support was used which was a solid welded support (support B) that bolted onto the turn-table limiting the rotation to a change in yaw angle. This stand was also made out of stainless steel and was very rigid.

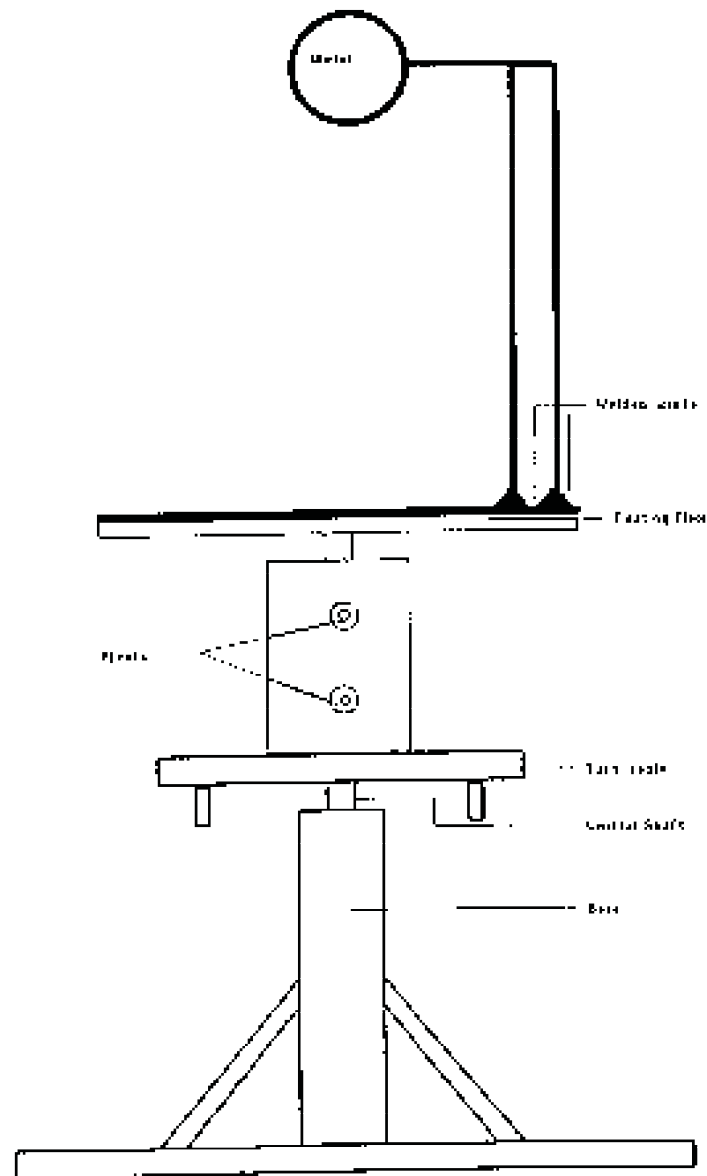


Fig 4.3. Schematic of Support B.

After the sting was sent in for repairs due to a faulty component, a further series of tests were carried out. This series only included tests of Lift and Drag variation with Yaw angle as these tests require all three force elements. For this type of test it is not possible to make use of only two components. A third support was used for this set of tests as the turn-table was already in use for other experimentation. This was also a welded support (support C) and was very rigid.

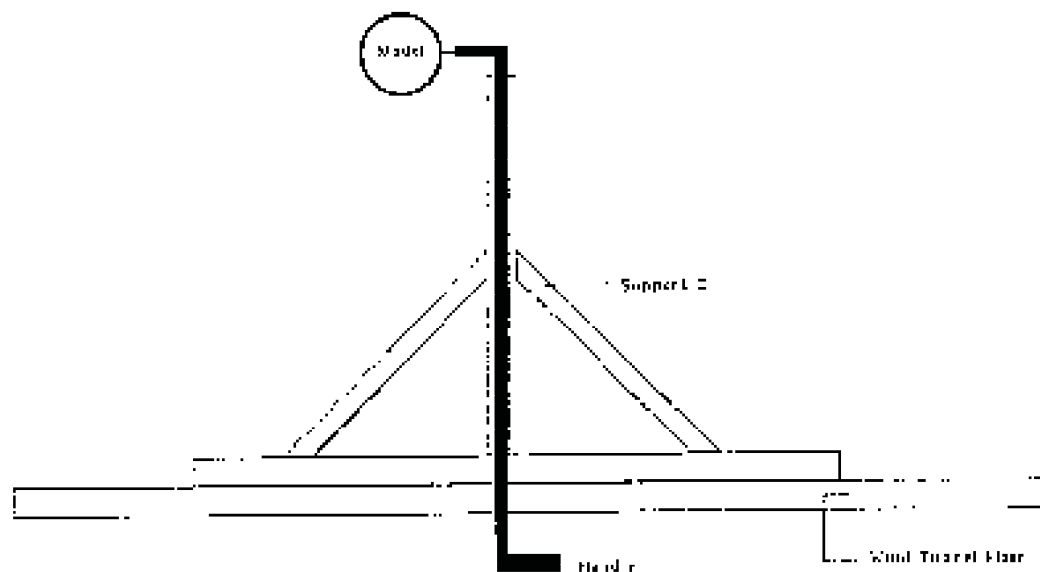


Fig 4.4. Schematic of Support C.

4.2 THE SIX COMPONENT STING BALANCE

A six component sting balance was used to measure the three forces and three moments. The reason for using a sting balance was two fold. Firstly, the sting could be narrow enough to cause the least interference in all measuring positions. Secondly, the model was very close to the virtual centre or position of measurement. This meant that the tare effects were minimal and if possible the centre of gravity of the model could be placed on the virtual centre. This would eliminate translation of the forces and moments from the virtual centre to the centre of gravity. The only transformation required would be to rotate the axes about the centre of gravity to obtain the output in terms of the wind axes.

The balance comprised two measuring sections contained within a 12 mm rod. The first section was the drag component unit. In this unit a beam was mounted transversely within the rod. When the balance was loaded in the drag direction, the beam was strained resulting in a moment which was then picked up by the strain gauges on the beam. The second section was where the other five components were measured. The centre of this section is called the virtual centre. This section comprised of four square beams with strain gauges mounted on them. The strain gauges were arranged such that four gauges make up a Wheatstone bridge and measure either force or moment.

The system was fitted with a Calwing. This is a resistor that electronically loads the bridge on the same leg with the same resistance before each test. Any system has a small drift with temperature and supply conditions. The drift is not only in the zero value but also affects the amplification factor. The drift in zero value was taken into account by the use of differential voltages. The change in amplification factor was taken into account by nondimensionalization. The nondimensional output is called a β factor and is defined below,

$$\beta = \frac{V - V_0}{V_{\text{calwing}} - V_0}$$

The other alternative was to re-calibrate the balance before each test. Each system is sensitive to temperature to a different degree and the resulting effects are different. Using the calwing method of artificial loading the output could be nondimensionalized by a constant loading condition.

The limit loads are:

$$\begin{aligned} X &= 25\text{N} \\ Y &= 100\text{N} \\ Z &= 100\text{N} \\ L &= 2\text{Nm} \\ M &= 8\text{Nm} \\ N &= 8\text{Nm} \end{aligned}$$

The mounting shaft had a diameter of 9 mm and a length of 30 mm. There were two ways of fixing the model to the balance:

- 1) An M4 screw fitted into the end of the shaft.
- 2) A 4 mm pin fitted through the mounting shaft half way along its length.

4.3 MODEL

The aerodynamic coefficients of a spinning sphere are relatively small when compared to those experienced by a wing or plate. In previous attempts to measure the aerodynamic forces on spinning spheres at The University of the Witwatersrand, no meaningful results were obtained. The model previously used was a steel sphere of ± 10 cm diameter. It was powered by a small DC motor. The author felt that the reason for not obtaining results was that the

model was far too heavy, resulting in high inertial effects, and that the surface area was far too small, resulting in small loads, for the sensitivity of balance used.

The model used in this experiment was made with an outside diameter of 22 cm. The sphere was made out of impregnated glass fibre and epoxy resin. The motor used to rotate the sphere was mounted inside the sphere in such a way that the motor was stationary and only the spherical shell rotated. This eliminated many balancing problems. The shell was constructed in two halves to facilitate repairs to the motor and the changing of the gearbox. There were four planetary gearboxes with a reduction ratio of 3, 4, 5 and 6. Two or more gearboxes could also be mounted on the motor at the same time resulting in a reduction factor of up to 360. The maximum rotational velocity obtained was 20 revolutions per second. This resulted in a maximum peripheral tangential velocity of 2.2 m/s. The total mass of the model was 1.5 kg. The models radial accuracy was well within 1%.

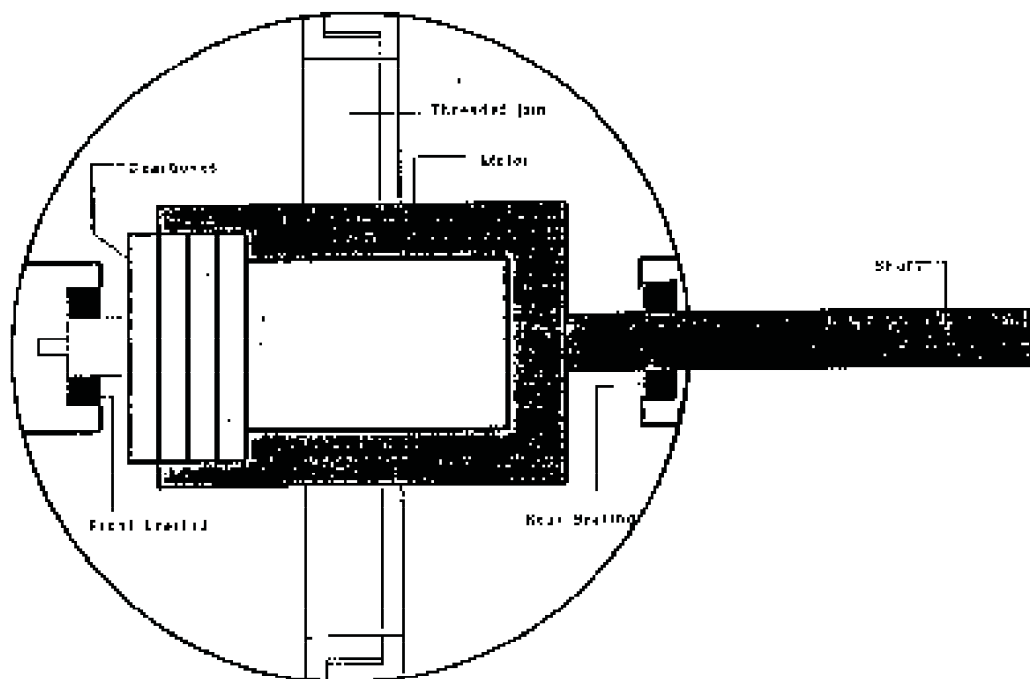


Fig 4.5. Schematic of Model Sphere.

4.4 DATA ACQUISITION SYSTEM

The data acquisition system consisted of an HBM UPM 60 unit linked to a personal computer via a serial interface. All the transducers were connected to the UPM 60 which took the readings and sent them to the computer.

There were various transducers linked to the UPM 60. There was a micro-manometer that measured the dynamic pressure, the six component sting balance described above, and a circuit that measured yaw and pitch angles.

The system can be operated by programs in any language that can control a serial communications port, but the following points should be remembered:

- 1) Compiled software runs much faster than uncompiled software.
- 2) The UPM 60 has a maximum baud rate of 19200 which is beyond the capabilities of a lot of compilers. This limit is a compiler limit not a language limit.

4.4.1 UPM 60

The UPM 60 is a multi point measuring device capable of processing and displaying 60 measured points from various detection devices. Measurements can be examined manually or automatically and fed to an output device. When taking measurements the unit makes use of all the preselected data for that particular channel eg. zero reading, bridge type, amplifier type, units and gauge factor.

When a reading is sent to the output device both the channel number and the units are sent with it. The output is usually displayed on the LED panel as well, unless the rate at which the channels are read is too fast for the display to register.

The UPM 60 can be programmed from both the front panel and the IEEE 488-78 interface. The RS 232-C interface has only been successfully used to transfer data from the unit to the computer, but it was not possible to programme the unit using the computer.

The unit has a built in thermal printer.

The unit also gives an option of four excitation settings:

- 1) 5 volt DC supply
- 2) 5 volt 225 Hz carrier frequency
- 3) 0.5 volt 225 Hz carrier frequency
- 4) 1 volt 5 kHz carrier frequency

The transducer readings are measured by means of a bridge circuit. These bridges are only energised when a measurement is being taken. The measured signal is then amplified and digitised before being fed into the internal computer for further processing should this be required.

Different scanning interfaces are available for the UPM 60 to allow for diversity in transducers that can be linked to the unit. There are four types of interfaces available for this unit.

- 1) Wheatstone bridge module
- 2) Voltage source ($\pm 100\text{mV}$) module
- 3) Voltage ($\pm 10\text{V}$) / Current ($\pm 20\text{mA}$) source module
- 4) Resistance module

The University only possesses the first three types.

There are two modules of type 1 enabling 20 channels of Wheatstone bridges to be connected to the unit. These bridges can consist of single strain gauges, half bridges or full bridge circuits. This is facilitated by means of an 'extended kreuzer circuit'.

There is one module of type 2. This can be used to input data from any other device that gives its output as a function of voltage in the range of ± 100 millivolts.

There is one module of type 3. This can be used when a device gives the output as a function of voltage and only uses the range ± 10 volts. The resolution of this module cannot be as fine as that of the previous module but the range is larger. This module can also be used for devices where the output is a function of current. The limiting current is 20 mA.

The analogue to digital converter is an integrator. This means that it integrates the incoming signal and divides by the duration of integration. This implies that the readings are effectively mean values. The duration of integration can be selected, with 4, 16, 20 or 100 milliseconds as the options available as the duration for integration.

4.4.2 COMPUTER

The computer used in this experiment was a personal computer of the XT variety with 640 kb of onboard memory. The computer was fitted with an RS 232-C serial interface. This was set to use a seven bit word with two stop bits and even parity.

4.4.3 SUPPLEMENTARY APPARATUS

One mercury thermometer with minimum and maximum values of -10°C and 50°C respectively and 1° increments

One Pitot tube that could reach beyond the boundary layer through the tunnel wall.

4.4.3.1 POWER SUPPLY

A regulated direct current power supply was used to drive the motor that rotated the sphere. It could deliver a maximum of 15 volts and 2 amps. It had a voltmeter and ammeter to show the output. The upper limit could be set for both the current and voltage. The unit was made by the KIKUSUI electronic corporation of Japan.

4.4.3.2 OPTICAL TACHOMETER

The optical tachometer was a hand held unit made by Ono Sokki, model number IIT-446. It relied on the reflection of an LED (light emitting diode) to determine the rotational velocity of its subject. For this reason a reflective strip was placed on the sphere. The unit has a range of 0.9 to 800 revolutions per second. The accuracy in the range from 0.9 to 200 RPS, which was the range in which the sphere was operating, was ± 0.02 RPS. The unit can operate in a temperature range of 0° to 40°C .

4.4.3.3 MICROMANOMETER

The micromanometer used was a Furness Control Limited model FCO 11. It had a range of ± 2000 Pascals. The unit also had an output socket that delivered one millivolt per Pascal.

5 THEORY

5.1 LIFT AND DRAG ON A SPINNING SPHERE

The theoretical prediction of lift on a sphere is complex and currently available models have proven to be not very accurate. The existence of lift on a spinning sphere can be explained by potential flow considerations (Davies 1949). If the spinning sphere is superimposed on the free stream velocity with the axis of rotation perpendicular to the free stream flow, the resulting velocity at a point is the sum of the component velocities. This implies that the velocity on one side of the sphere is the sum of the two velocities, and on the other it is the difference. From Bernoulli's equation it can be shown that as the velocity of a fluid increases the pressure decreases. This implies that the pressure on the side where the velocity is increased has a lower pressure than the side with the decreased velocity. This difference in pressure results in a net force being exerted on the sphere.

The theory of a spinning cylinder shows that the lift is a function of the free stream velocity, the density and the circulation. (Houghton 1982)

$$L = \rho U \Gamma$$

The tangential velocity gives the circulation in terms of rotational velocity and radial length.

$$V_{\theta} = \omega r = \frac{\Gamma}{2\pi r}$$

$$\Gamma = 2\pi \omega r^2$$

If the above equation is substituted into the lift equation and nondimensionalized to give the coefficient of lift we get:

$$C_L = \frac{2\pi \omega r}{U}$$

If we then define the nondimensional spin parameter or velocity ratio as

$$\alpha = \frac{\omega r}{U}$$

then for a given cylinder the relationship between the coefficient of lift and the nondimensional spin parameter should be linear.

For this reason the spin was nondimensionalized in this way.

For a sphere it is not as simple to find a relationship for lift using potential flow theory. The equation given below was derived using Stokes solution with an Oseen expansion of the Navier-Stokes equations (Rubinow 1964). These two approximations are limited to low Reynolds numbers.

For a sphere the formulae for lift and drag are:

$$C_L = 2\alpha [1 + O(Re)]$$

$$C_D = \frac{32\mu}{\rho U_\infty r} \left[1 + \frac{3}{8} Re + o(Re) \right]$$

5.2 STING BALANCE

The balance to be considered is a six component sting balance with a four beam cage to measure the last five components and a single beam to measure the first component.

The theory is based on that for measuring the normal force and moment applied to a cantilever. The cantilever is fitted with four strain gauges as shown in the following diagram.

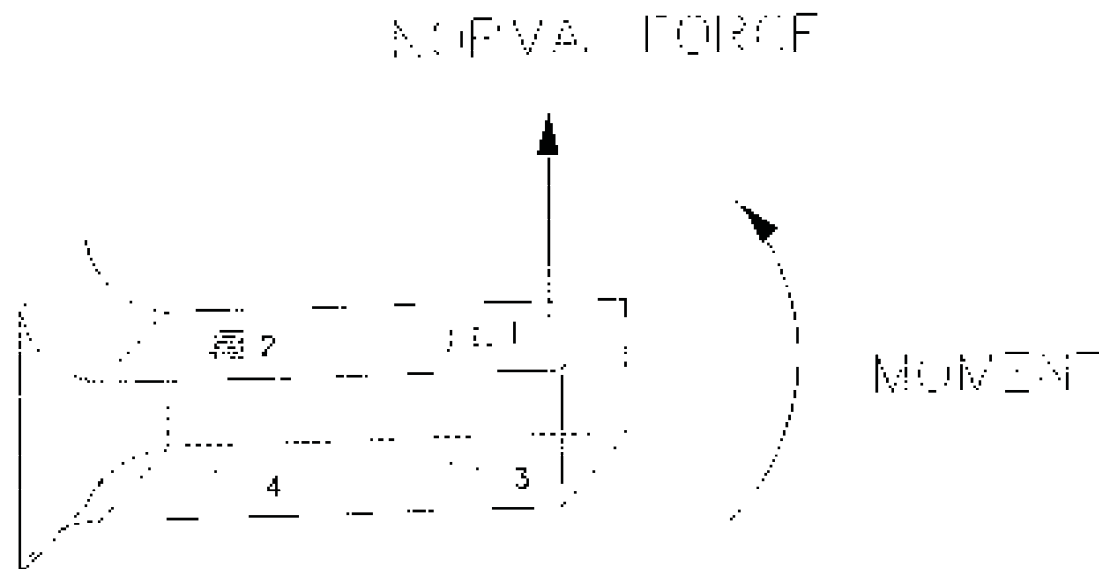


Fig. 5.1. Layout of strain gauges on a cantilever sensitive to normal forces and moments.

The stress in a beam is given by:

$$\sigma = \frac{My}{I}$$

Where M is the applied moment

y is the distance from the neutral axis to the position in question

I is the second moment of area

It is also known that the strain is linearly proportional to the applied stress within the elastic limits. Therefore the strain is linearly proportional to the applied load.

The strain gauges are connected in the form of a Wheatstone bridge as shown below:

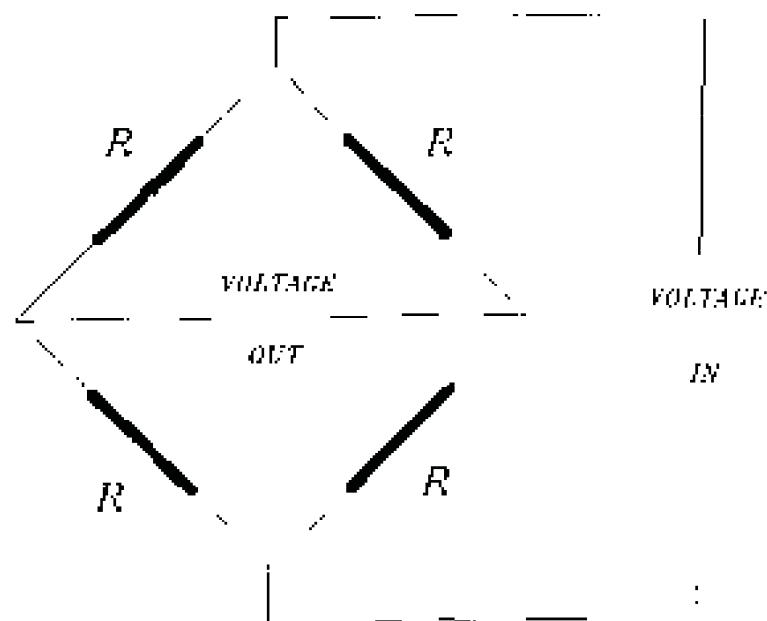


Fig. 5.2. Layout of Wheatstone bridge circuit.

The voltage out is proportional to the difference in strains of the gauges in adjacent legs and to the sum of the strains in gauges located in opposite legs.

The bridge configuration shown below is sensitive only to normal forces in the plane of the strain gauges and unaffected by other applied loads.

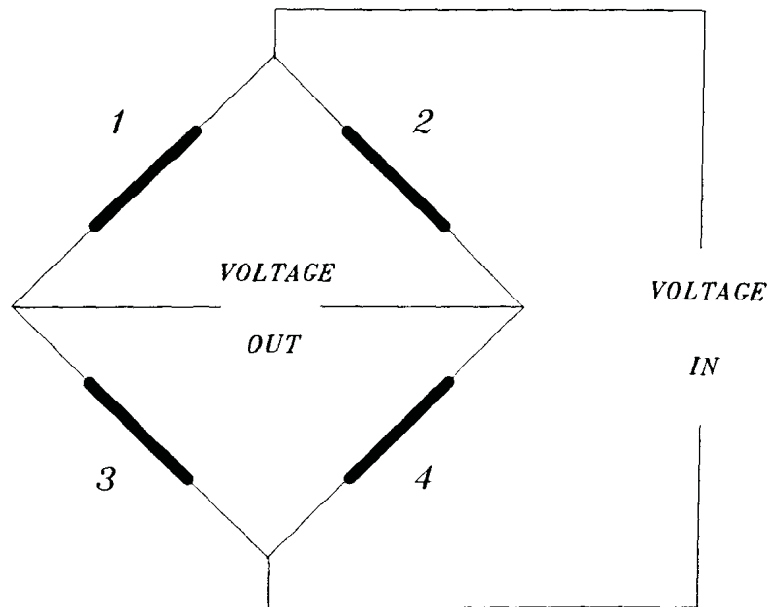


Fig. 5.3. Layout of Wheatstone bridge circuit sensitive to normal forces (the numbers correspond to those in Fig 9.1).

The bridge configuration shown below is sensitive only to moments in the plane of the strain gauges and insensitive to other loads.

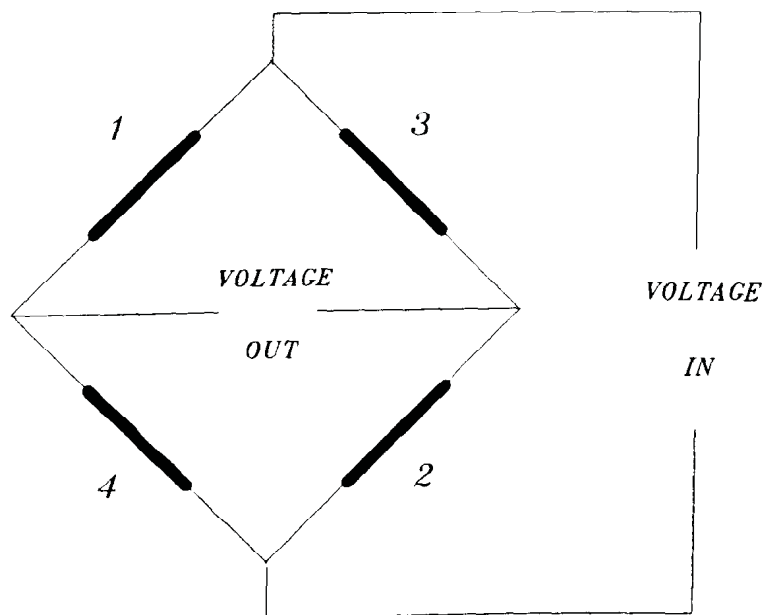


Fig. 5.4. Layout of Wheatstone bridge circuit sensitive to moments only (the numbers correspond to those in Fig 9.1).

Based on this theory the Y and Z forces and the M and N moments can be determined. The X component can be determined if a force sensitive configuration is used with a beam mounted perpendicular to the axis of the balance.

This leaves the rolling moment or L moment. The diagram below shows the cantilever configuration for this moment.

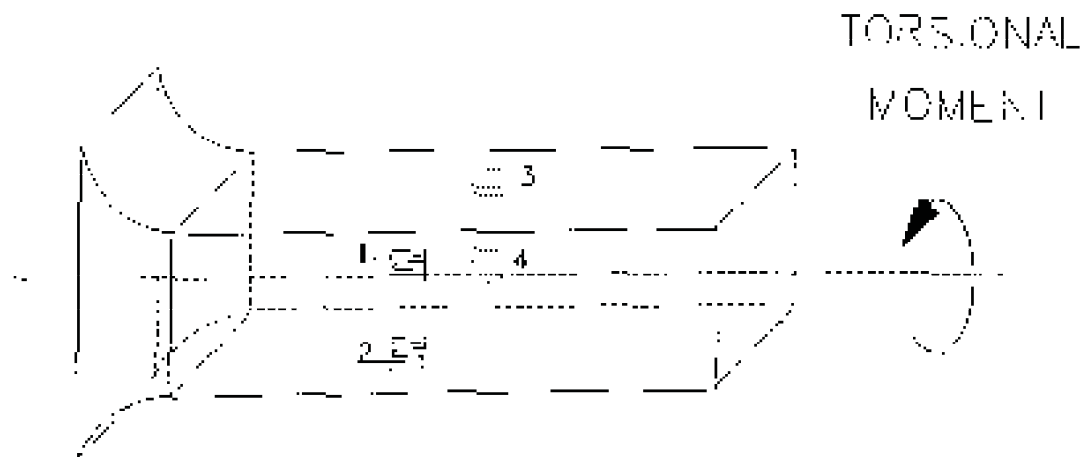


Fig. 5.5. Layout of strain gauges on a cantilever sensitive to rolling moment.

If the strain gauges are connected as follows then the bridge will be sensitive only to the rolling moment.

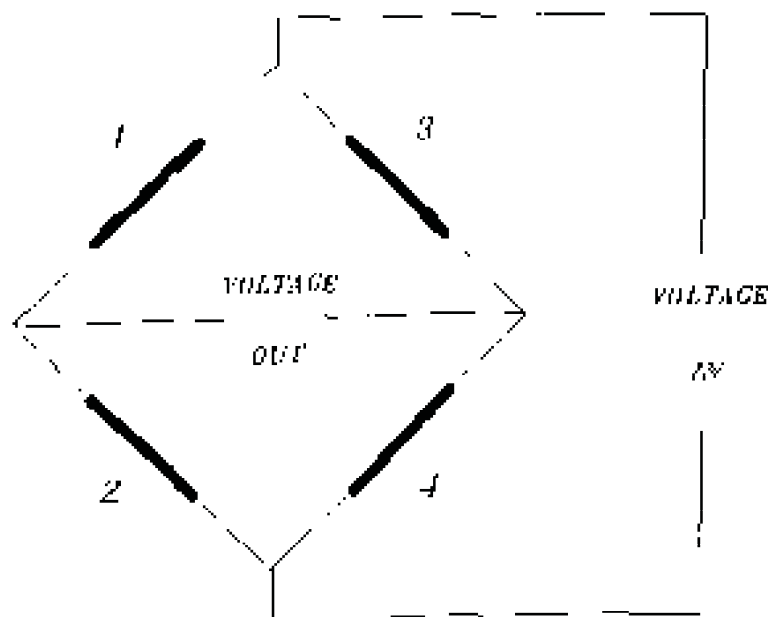


Fig. 5.6. Layout of Wheatstone bridge circuit sensitive to rolling moment only (the numbers correspond to those in Fig 9.1).

5.3 NONDIMENSIONALIZATION AND CALIBRATION EQUATIONS

To allow for the most versatility the variables are nondimensionalized. This makes them independent of the system of units used. To add further versatility to the system the output is made independent of the input voltage in the following manner

$$V = \frac{OUTPUT \ VOLTAGE \ (microvolts)}{INPUT \ VOLTAGE \ (volts)}$$

The output is then converted to strain using a gauge factor of two defined as follows

$$k_E = \frac{S_k}{S_N} \cdot A_G$$

k_E = scale factor to be selected

S_N = nominal output of transducer in mV/V (2000 $\mu\text{m/m}$ = 1 mV/V)

S_k = control signal of the selected excitation in mV/V.

$$\begin{aligned} \text{for } 225 \text{ Hz} &= 2\text{mV/V} \\ 5 \text{ kHz} &= 80\text{mV/V} \\ \text{DC} &= 20\text{mV/V} \end{aligned}$$

A_G = required indication in digit. (Nominal)

This results in the output have the units of $\mu\text{m/m}$.

To allow the balance to be used on any data acquisition system without re-calibration the output is converted to β factors. This eliminates any errors due to tolerances between systems. β is defined as:

$$\beta = \frac{V - V_0}{V_{\text{calibrating}} - V_0}$$

Where the voltage indicated here is the output voltage from the data acquisition system.

The relationship between the β factors and the load is :

$$[\beta_1 \beta_2 \beta_3 \beta_4 \beta_5 \beta_6] \begin{bmatrix} C_{11} & C_{12} & C_{13} & C_{14} & C_{15} & C_{16} \\ C_{21} & C_{22} & C_{23} & C_{24} & C_{25} & C_{26} \\ C_{31} & C_{32} & C_{33} & C_{34} & C_{35} & C_{36} \\ C_{41} & C_{42} & C_{43} & C_{44} & C_{45} & C_{46} \\ C_{51} & C_{52} & C_{53} & C_{54} & C_{55} & C_{56} \end{bmatrix} = \begin{bmatrix} X \\ Y \\ Z \\ I \\ M \\ N \end{bmatrix}$$

5.4 TRANSFORMATION FROM BALANCE AXES TO WIND AXES AT CENTRE OF GRAVITY

5.4.1 TRANSLATION OF MEASURED LOADS TO THE CENTRE OF GRAVITY OF THE MODEL

$$X_B = X_S$$

$$Y_B = Y_S$$

$$Z_B = Z_S$$

$$L_B = L_S$$

$$M_B = M_S + Z_S \times c_G$$

$$N_B = N_S - Y_S \times c_G$$

5.4.2 ROTATION OF MEASURED LOADS TO WIND AXES

$$\begin{bmatrix} X_W \\ Y_W \\ Z_W \end{bmatrix} = \begin{bmatrix} \cos(ATTACK)\cos(YAW) & -\sin(YAW) & \sin(YAW)\cos(ATTACK) \\ \cos(ATTACK)\sin(YAW) & \cos(YAW) & \sin(ATTACK)\sin(YAW) \\ -\sin(ATTACK) & 0 & \cos(ATTACK) \end{bmatrix} \begin{bmatrix} X_B \\ Y_B \\ Z_B \end{bmatrix}$$

$$\begin{bmatrix} L_W \\ M_W \\ N_W \end{bmatrix} = \begin{bmatrix} \cos(ATTACK)\cos(YAW) & -\sin(YAW) & \sin(YAW)\cos(ATTACK) \\ \cos(ATTACK)\sin(YAW) & \cos(YAW) & \sin(ATTACK)\sin(YAW) \\ -\sin(ATTACK) & 0 & \cos(ATTACK) \end{bmatrix} \begin{bmatrix} L_B \\ M_B \\ N_B \end{bmatrix}$$

5.5 LEAST SQUARES APPROXIMATION OF A THIRD ORDER POLYNOMIAL

The least squares approximation is used to fit a curve to a set of data points with as little error as possible. In this case a third order polynomial is required to fit data so that the function value can be obtained for any value of the independent variable within the range for which data is available.

$$\begin{bmatrix} m & \sum x_i & \sum x_i^2 & \sum x_i^3 \\ \sum x_i & \sum x_i^2 & \sum x_i^3 & \sum x_i^4 \\ \sum x_i^2 & \sum x_i^3 & \sum x_i^4 & \sum x_i^5 \\ \sum x_i^3 & \sum x_i^4 & \sum x_i^5 & \sum x_i^6 \end{bmatrix} \begin{bmatrix} A_0 \\ A_1 \\ A_2 \\ A_3 \end{bmatrix} = \begin{bmatrix} \sum y_i \\ \sum x_i y_i \\ \sum x_i^2 y_i \\ \sum x_i^3 y_i \end{bmatrix}$$

Where m is the number of data points.

This results in an equation of the form :

$$y = A_0 x + A_1 x + A_2 x^2 + A_3 x^3$$

6 CALIBRATION

During testing the zero reading was subtracted from any reading before the reading was manipulated. The reason for this was to eliminate any zero offset. This is the usual practice since the zero setting can change from test to test due to voltage drift in the acquisition system, different configurations of model, and atmospheric conditions. This also simplifies any data manipulation because if the relationship between load and output is linear then the voltage difference need only be multiplied by the gradient and the constant can be ignored. This may appear insignificant but when manipulating large matrices it can save time and bother.

6.1 CALIBRATION OF SIX COMPONENT STING BALANCE

The calibration was carried out to generate a 6×6 matrix that would take into account any linked effects that occurred in the balance. This was achieved by loading the balance in one plane only at a time. The balance was loaded and the output measured. Care was taken to see that there was no misalignment in the loading. It was found that the presence of pulleys caused a great deal of error in both alignment and loading values due to friction. For this reason it was decided to eliminate pulleys from the calibration completely. This was achieved by rotating the sting so that the axis along which the load was to be applied was pointing vertically downward. A jig was built to hold the sting in position limiting the misalignment.

When the balance was placed in the jig pointing vertically downwards the drag component could be calibrated simply by hanging known loads on the end of the sting. A series of tests was run with various loading conditions.

The balance was then set up to point horizontally, in the manner that it stands in the wind tunnel. Here the procedure was a little more complicated. If the load is applied at the centre of the strain gauges in the Z direction only a force is applied and the associated moment is zero. This was done to calibrate lift.

While the balance was in this position the pitching moment could also be calibrated by moving the point of application of the load away from the centre of the strain gauges along the X axis or shaft of the balance. It is advisable to change the applied moment by both increasing the load as well

as increasing the distance between the point of application and the centre of the strain gauges. This procedure was followed to calibrate pitching moment.

The rolling moment was also calibrated while the balance was in this configuration. This was achieved by moving the point of application away from the strain gauges along the Y axis or perpendicular to the axis of the balance in the horizontal plane. Once again it is suggested that both the distance and the load are changed to vary the applied moment.

The balance was then placed on its side in the jig with the positive Y axis in the vertically downward position. In this position the side force could be calibrated when the point of application coincided with the centre of the strain gauges. The balance was loaded with different mass pieces. The point of application was then moved along the axis of the balance to apply a yawing moment. Here too the distance as well as the load was varied.

The output from all the tests were put into one worksheet with a column for each component. These columns are labelled β_1 to β_6 and the corresponding loads were placed in the six columns following. It must be remembered that the balance was also loaded with a force when calibrating the three moment components.

The worksheet was then put through a multiple linear regression. This process finds the solution to the following equation:

$$(\beta_1 \quad \beta_2 \quad \beta_3 \quad \beta_4 \quad \beta_5 \quad \beta_6)(C_1 \quad C_2 \quad C_3 \quad C_4 \quad C_5 \quad C_6) = (LOAD)$$

This implies that the solution to only one loading case could be found at a time. Therefore the applied forces X, Y, and Z and moments L, M, and N were substituted into the variable called load. The values of C were then substituted into a matrix row by row to give a full calibration matrix, satisfying the following equation.

$$[\beta_1 \beta_2 \beta_3 \beta_4 \beta_5 \beta_6] \begin{bmatrix} C_{11} & C_{12} & C_{13} & C_{14} & C_{15} & C_{16} \\ C_{21} & C_{22} & C_{23} & C_{24} & C_{25} & C_{26} \\ C_{31} & C_{32} & C_{33} & C_{34} & C_{35} & C_{36} \\ C_{41} & C_{42} & C_{43} & C_{44} & C_{45} & C_{46} \\ C_{51} & C_{52} & C_{53} & C_{54} & C_{55} & C_{56} \\ C_{61} & C_{62} & C_{63} & C_{64} & C_{65} & C_{66} \end{bmatrix} = \begin{bmatrix} X \\ Y \\ Z \\ L \\ M \\ N \end{bmatrix}$$

The calibration carried out initially (referred to as position 1) showed that the Z component had a tendency to shift its zero if the balance was physically moved, even if this was only to change the angles of attack or yaw.

For this reason the tests were repeated with the sting rotated through 90° (referred to as position 2). This meant that the faulty component was used to measure side force and not lift.

This is the calibration matrix for the sting in position 1. The output from Statgraphics can be seen in Appendix B.

$$\begin{bmatrix} 0.043029 & 0.000107 & 0.001265 & 0.001118 & 0.000976 & -0.010311 \\ 0.000153 & 0.005393 & -0.07618 & 0.004616 & -0.001104 & -0.004387 \\ -0.0000613 & 0.077882 & -0.010820 & 0.007902 & 0.000114 & 0.003223 \\ 0.000001 & -0.000070 & 0.000042 & -0.00293 & -0.000139 & 0.000135 \\ -0.000017 & 0.000006 & 0.000001 & 0.00004 & -0.000072 & -0.004647 \\ 0.000014 & -0.000017 & 0.000064 & 0.000087 & 0.004763 & 0.00005 \end{bmatrix}$$

This is the calibration matrix for the sting in position 2. The output from Statgraphics can be seen in Appendix B.

$$\begin{bmatrix} -0.043476 & 0.001627 & 0.001097 & 0.001549 & 0.002251 & -0.003134 \\ -0.000148 & 0.000851 & -0.000014 & 0.000261 & 0.006639 & -0.002155 \\ -0.00005 & -0.007446 & 0.075435 & -0.000081 & -0.000531 & 0.005803 \\ -0.000001 & 0.000072 & 0.000151 & -0.002952 & -0.000098 & 0.000158 \\ 0.000045 & 0.000001 & 0.000009 & 0.000113 & 0.004758 & 0.000088 \\ 0.000066 & 0.000002 & -0.000020 & -0.000092 & -0.000020 & 0.004602 \end{bmatrix}$$

After the tests were carried out the sting was sent in for repairs and another calibration was carried out.

This is the calibration matrix for the sting in position 2 after repairs. The output from Statgraphics can be seen in Appendix B.

$$\begin{bmatrix} -0.043421 & 0.002771 & 0.002477 & 0.000461 & 0.001929 & -0.002981 \\ -0.000072 & 0.070135 & 0.005213 & 0.005393 & 0.001262 & 0.009355 \\ 0.000231 & -0.010285 & 0.077193 & -0.000185 & 0.000397 & 0.002133 \\ 8.101009E-6 & 0.000501 & -0.000305 & 0.005103 & 0.000139 & -0.000372 \\ 0.00003 & -0.000974 & 0.007265 & -0.000488 & 0.004606 & 0.000663 \\ 0.000074 & -0.006578 & 0.000173 & -0.000545 & -0.000233 & 0.003718 \end{bmatrix}$$